Structure and Electrophysical Properties of Double-component Film Alloys Based on Molybdenum and Iron or Nickel

I.P. Buryk, T.M. Hrychanovs'ka, D.V. Poduremne, A.O. Stepanenko

Sumy State University, Rymskyi-Korsakov Str., 2, 40007 Sumy, Ukraine

The study of the structure-phase composition and electrophysical properties of film alloys of molybdenum and nickel or iron were deposited by the method of simultaneous thermo-vacuum condensation was done. In a non-annealing state, the samples remain biphasic. After heat treatment at 750 K in vacuum, the formation of the metastable phases of the fcc-Ni$_3$Mo (lattice parameter $a = 0.360$ nm) and bcc-Fe$_2$Mo ($a = 0.296$ nm) in film alloys based on Ni and Mo was recorded at concentrations of atoms of ferromagnetic metal 75 and 65 at.% respectively Investigation of the thermoresistive properties of films showed that the dispersion of the structure, the admixture phases and the solid phase reactions affect the temperature dependence of the resistivity and the temperature coefficient of resistance. In film alloys, the range of elastic deformation remains greater than several times than for single-layer metal films, while the strain coefficient is practically unchanged.

Keywords: Double-component film alloys, Structure-phase state, Theroresistive effect, Strain effect.

1. INTRODUCTION

The physico-mechanical, electrophysical and magnetoresistive properties of film alloys are of particular interest to researchers. The search for new materials with high durability, thermal stability, catalytic activity and other characteristics led to the synthesis of double-component film alloys of molybdenum and nickel or iron [1-6]. According to [7, 8], in the Ni-Mo system, the formation of three equilibrium ordered intermetallic phases (β-Ni$_4$Mo, γ-Ni$_3$Mo and δ-NiMo) is possible. At elevated temperatures, the Ni$_3$Mo alloy splits into two metastable phases of Ni$_2$Mo and Ni$_4$Mo. In [8] the possibility of formation of a metastable phase of Ni$_8$Mo is considered. The temperatures at which the Ni$_8$Mo, Ni$_4$Mo, Ni$_3$Mo, Ni$_2$Mo and NiMo phases are stabilized 555, 1148-1150, 1200, 1033-1073 and 1619 K [8] respectively. According to the state diagram in the Fe-Mo system, four intermediate phases (δ-FeMo, μ-Fe$_7$Mo$_6$, R-Fe$_{62}$Mo$_{38}$, λ-Fe$_2$Mo) and solid solutions based on α-Fe and γ-Fe are possible. The maximum solubility of Fe in Mo at temperatures of 1813 K and 1508 K is about 22 and 6 at. % The maximum solubility of Fe in Mo occurs at a temperature of 1884 K is 31.3% and at 1508 K – 6.2%. Parameter lattice fcc-Fe and solid solutions (s.s.) based on Fe and Mo with a molybdenum concentration of 2.4; 4.2; 11.0 and 12.6 at. % is 0.287; 0.288; 0.282; 0.290 and 0.291 nm respectively.

Consequently, the analysis of previous studies has shown that the structural and electrophysical properties of Ni$_x$Mo$_{1-x}$ and Fe$_x$Mo$_{1-x}$ film alloys in the field of low and intermediate temperatures remain poorly understood today. The results obtained in the work for double-component film alloys can be used in the development of metal-film strain sensors and thermistors, pressure sensors with stable operating characteristics.

2. EXPERIMENT TECHNIQUE

Film alloys Ni$_x$Mo$_{1-x}$ and Fe$_x$Mo$_{1-x}$ were obtained by simultaneous thermal-vacuum condensation with electron beam (Mo) and resistive (Ni, Fe) evaporation in vacuum device VUP-5M (pressure $10^{-3} - 10^{-4}$ Pa). The main technological parameters were: average condensation velocity (ω), substrate temperature and annealing temperature. The speed of condensation was ω(Ni, Fe) $\cong 1,0$ nm/s and ω(Mo) $\cong 0.3 - 0.4$ nm/s. The substrate temperature ($T_s \cong 300$ K) and annealing ($T_{an} \cong 750$ K) were constant and determined the formation of the films microstructure. Annealing time was $t = 15$ min.

The film thickness was controlled by the quartz resonator method. Structural and diffraction studies were held on device TEM-125K («Selmi», Sumy).

The concentration of individual components was estimated by the ratio:

$$c_i = \frac{\rho_i d_i \mu_i^{-1}}{\sum\limits_{i=1}^{n} \rho_i d_i \mu_i^{-1}},$$

where ρ_i, d_i and μ_i - density, thickness and molar mass of individual components.

Based on the temperature dependence of the resistivity (ρ) (II temperature cycle at the cooling) calculated thermal coefficient of resistance (TCR) base on ratio

$$\beta = \frac{\rho(T) - \rho(300)}{\rho(300)(T - 300)}.$$

The longitudinal strain coefficient (γ_l) was calculated by the angular strain coefficient dependence $\Delta R/R(0)$ versus ε_l based on ratio:

$$\gamma_l = \frac{R(\varepsilon_l) - R(0)}{R(0)} \cdot \frac{1}{\Delta \varepsilon_l},$$

where $R(\varepsilon_l)$ and $R(0)$ —the final and initial resistance;

$\Delta \varepsilon_l = \Delta l / l_i$ − longitudinal strain (l_i − initial sample length).

3. STRUCTURE AND PHASE COMPOSITION

Consider the results of electron and electron-microscopic studies of film alloys on the basis of *a*-Mo (*a*-amorphous phase) and metal components of fcc-Ni or bcc-Fe of different concentrations.

On a didffraction patter (Fig. 1a) for a non-annealing film alloy based on Ni and Mo ($c_{Ni} \cong$ 75 at. %, $c_{Mo} \cong$ 25 at. %), lines from the crystallographic planes of the fcc-phase Ni with a crystalline lattice parameter is approximately 0,351 nm are fixed. This value indicates that the Mo atoms are almost insoluble in the hcc-Ni lattice and are likely to be localized on the grain boundaries in the amorphous state.

After vacuum heat treatment for 15 minutes at the $T_в \cong$ 750 К near diffraction rings belonging to the fcc-Ni, the formation of new diffraction rings of a slightly smaller diameter (Fig. 1c). They observed, which correspond to the crystallographic planes (111), (200), (220) and (311) with interplanar distances of 0,208; 0.180; 0.127 and 0.108 nm, such as for intermetallic $Ni_{75}Mo_{25}$ ($a = 0.360$ nm) [7]. The authors [7] note the correspondence of experimental data to the estimated data obtained under the Vegard rule. At the same time, they used a value of the lattice parameter 0.385 nm for the metastable fcc-phase Mo. If in the latter case take a value 0.397 nm [9], then the calculated value of the lattice parameter for the Ni_3Mo alloy will be about 0.336 nm.
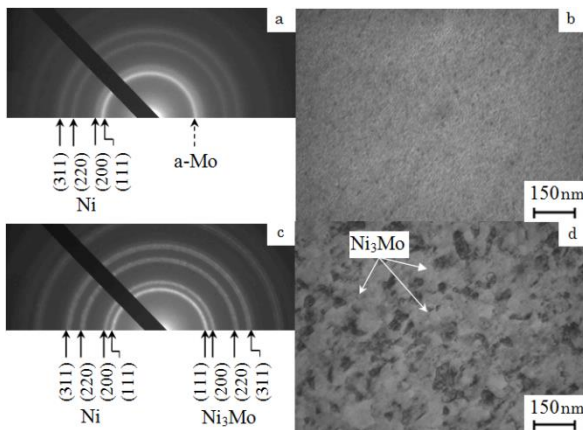
Fig. 1 – Diffraction patterns and microstructure from Ni + Ni_3Mo film (comon thickness – 30 nm) after deposition (a, b) and heat treatment at the $T_{an} \cong$ 750 К (c, d)

Along with this study [10] showed that after pressing the nanocomposite $Ni_{80}Mo_{20}$ had a crystalline structure with a latticeparameter 0.361 nm. We note that for a(Mo) = 0,397 nm [9]] for $Ni_{80}Mo_{20}$, the calculation of the magnitude of the lattice parameter according to Vegard's rule gives a similar result. After thermomechanical processing of nanocomposites $Ni_{80}Mo_{20}$ and $Ni_{57}Mo_{43}$ at 1473 K [10] formation of Ni_4Mo and MoO_2. was observed. The study of the phase composition of Ni-Mo-O electrochemical coatings was carried out in [11], and it was found that at concentrations of Ni and M atoms near 3: 1 the Ni_4Mo, MoO_3 and NiO phases are observed.

Thus, the formation of new diffraction rings can be linked to the formation on the basis of a crystal lattice Ni of a new fcc-phase. In this case, the formation of metastable intermetallic Ni_3Mo and Ni_4Mo, is equally possible, which is consistent with the Ni-Mo state diagram. We note that for both cases, limited areas of homogeneity are characteristic. It is also known (see, for example, [12]) that the fcc-phase which take place for NiO, but in this case the lattice parameter is 0.418 nm.

Consider the diffraction patterns obtained for the $Ni_{75}Mo_{25}$ film before and after the heat treatment. For a us-deposition sample, a nanodisperse structure (Fig. 1b) is fixed with an average grain size near 10 nm. It should be noted that crystallites and their boundaries are saturated with atoms of impurities already at the condensation stage. What is evident from the blurring of the lines (Fig. 1a). After annealing, a typical structure for Ni-polycrystalline film is formed (see Fig. 1d). Between small crystallites it is possible to see considerably larger ones which were formed as a result of recrystallization processes. The average grain size is 40 nm. However, in a microphoto it is possible to single crystallites, which have dark and light contrasts. Light grains of the pentagonal form belong to the metastable fcc-phase of Ni_3Mo, while the dark ones are the fcc-phase Ni.

As an example in Fig. 2 results of diffraction and electron microscopic studies of phase composition and crystalline structure of films based on Ni and Mo ($c_{Ni} \cong$ 65 at. %, $c_{Mo} \cong$ 35 at. %) us-deposition and after heat treatment are given. In non-annealed samples, the diffraction rings are fixed from the crystallographic planes of the fcc-Ni (111), (200), (220) and (311) with corresponding interplanar distances of 0.204, 0.176, 0.125 and 0.106 nm, and two weak lines belonging to the impurity fcc-phase $Mo(C,N)_x$ (Fig. 2a).

Heat treatment at the $T_{an} \cong$ 750 К leads to the fact that the diffraction maxima become more precise. After heat treatment, an increase in the crystal lattice parameter from 0.352 to 0.357 nm for the fcc-Ni phase is observed. This is due to the penetration of impurity atoms into crystal lattice Ni. Thus, in this case, the formation of eutectic based on fcc-phase Ni is fixed. Mo residues are used to form the impurity fcc-phase $Mo(C,N)_x$. On the diffraction patterns (Fig. 2b) there is a blur of lines (111) and (220) with corresponding interplanar distances 0.242 and 0.149 nm corresponding to the crystallographic planes of the fcc-phase $Mo(C,N)_x$. This is probably due to the fact that as a result of thermodiffusion, the impurity atoms, segregated at the grains boundaries, penetrate into their bulk.

Like the case discussed above, the image of the surface of the us-deposited and annealed films is significantly different. In non-anneled films, a fine-dispersed microstructure is fixed (Fig. 2b), while at annealed − typical structure for polycrystalline films (Fig. 2d). The average size of grains for films before and after heat treatment is respectively 10 and 25 nm. Thus, an increase of the Mo atoms concentration of leads to a decrease in the average size of grains in film
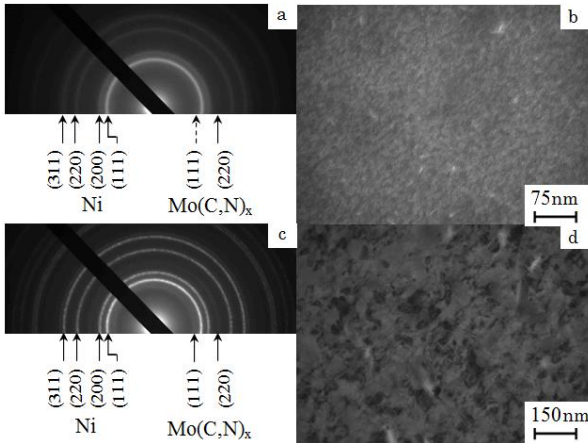
Fig. 2 – Diffraction patterns and microstructure from heterogeneous film ($d \cong 30$ nm) us-deposited (a, b) and annealed at the $T_{an} \cong 750$ К (c, d)

Fig. 3 – Diffraction patterns and microstructure from heterogeneous film based on Ni ($d \cong 30$ nm) us-deposited (a, b) and annealed at the $T_{an} \cong 750$ К (c, d)

alloys in annealed state. We note that in this case the phase composition of the unabsorbed sample corresponds to the phase composition of the annealed sample.

In Fig. 3 shows the results of diffraction and electron microscopy studies for film alloys based on Fe and Mo ($c_{Ni} \cong 65$ at. %, $c_{Mo} \cong 35$ at. %) us-deposition and after heat treatment. The diffraction rings are clearly observed on the electron graph (Fig. 3a) from the crystallographic planes bcc-Fe (110), (200) and (211) with corresponding interplanar spacings of 0,202, 0,143 and 0,117 nm, and a very weak blurred line from a-Mo.

A similar situation is observed in double-layer Fe/a-Mo/S (S - substrate) films deposited by the method of layer condensation [13]. After annealing to a temperature of 750 K and cooling to room temperature in a diffraction pattern (Fig.3b), along with the lines of the bcc-Fe phase are new ones that correspond to the metastable bcc-Fe₂Mo phase (200) and (222) with corresponding interplanar distances of 0.148 and 0.124 nm, oxide Fe₃O₄ (311), (422) and (533) with corresponding interplanar distances 0.254, 0.172 and 0.128 nm, and fcc-Mo (110) – 0.224 nm. It is known [13-15] that the active interaction of Fe atoms with oxygen at intermediate annealing temperatures in the technological vacuum generally results in the formation of oxides Fe₃O₄ and Fe₂O₃.

In a non-annealing state, film alloys based on Fe and Mo ($c_{Fe} \cong 75$ at. %) had a dispersed structure with an average crystallite size of 10 nm (Fig. 1b) and 30 nm after heat treatment (Fig. 1d).

We note that in [6] the authors the results obtained by the methods of transmission electron microscopy and computer simulation, which show that the annealing of Fe₈₀Mo₂₀ alloys for 20 hours at a temperature of 773 K causes self-organization processes, which leads to formation in the matrix Fe directed nanosilver enriched by Mo atoms. Calculated values of the crystalline lattices parameters of confirm this conclusion. It also fixes the formation of impurity phases Mo(C,N)ₓ, Fe₃O₄ and Fe₂O₃, which is associated with active interaction with the atoms of residual gases during condensation andannealing of samples. In the
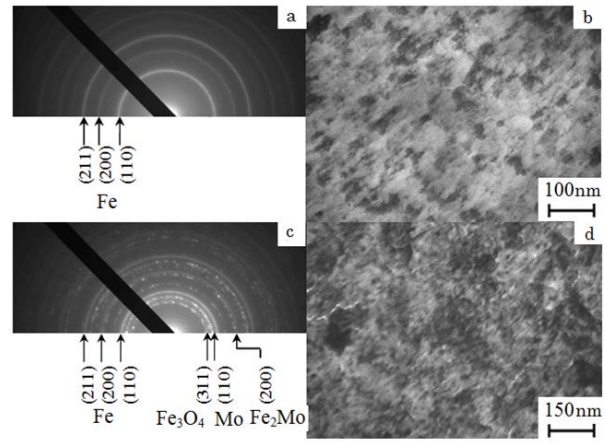
double-layer film systems Fe/a-Mo/S [13] obtained by layer condensation, we observed the individual identity of individual components with annealing up to 800 K.

4. ELECTROPHYSICAL PROPERTIES

In Fig. 4a, b, the typical strain dependences for film samples based on Ni and Mo ($c_{Ni} \cong 65$ at. %) and Fe and Mo ($c_{Fe} \cong 65$ ат. %) with thickness 30 nm are shown. On the whole strain interval, the samples remained elastic (Fig. 4), and the value of the of strain coefficient (CT) was 6.0 and 4.7 units, strain sensitivity of the resistivity is $5 \cdot 10^{-4}$ Ohm m/%. Thus, the strain properties of film alloys remain similar to heterogeneous films [13].

It is known that the transition elastic/plastic strain is accompanied by a change of angle inclination of strain dependences. We note that in single-layes films of the same thickness Mo, Fe and Ni, the longitudinal strain of the transition $\varepsilon_{ltr} \cong 0.22$; 0.30 та 0.16 % respectively. At the same time, in the films based on Ni and Mo or Fe and Mo, the strain transition lies outside $\varepsilon_l \cong 1$ % which is due to the peculiarities of their
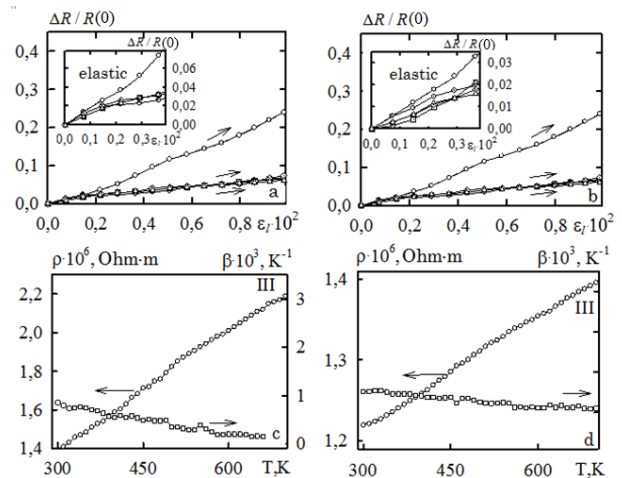
Fig. 4 – Strain (a, b) and temperature (c, d) dependences for heterogeneous films fcc-Ni + Mo(C,N)ₓ (a,c) and bcc-Fe + Fe₂Mo + Fe₃O₄ (b, d)]

structure. The TCR calculation based on the temperature dependence of the resistivity show that its value $(1.2-2.2) \cdot 10^{-3}$ K^{-1} has a typical value for the heterogeneous film materials.

5. CONCLUTIONS

Electron and electron microscopy studies of alloy Ni and Mo or Fe and Mo alloy films that were deposited by simultaneous condensation were carried out. In us-deposition state, the samples remain biphasic.

The diffraction maxima from the crystallographic planes of the metal components fcc-Ni or bcc-Fe and a- Mo are fixed. In the vacuum heat treatment up to 750 K, peculiarities of the phase composition formation of film alloys were determined.

In films based on Ni and Mo at a concentration of $c_{Ni} \cong 75$ at. % on diffraction patterns the system of lines is fixed from two fcc lattices that correspond to fcc-Ni ($a = 0.352$ nm) and metastable fcc- Ni$_3$Mo ($a = 0.360$ nm). For $c_{Ni} \cong 65$ at. % fixed the lines that corresponded to the fcc-phases of Ni and Mo(C,N)$_x$ with lattice parameters 0.357 and 0.419 nm, which is due to penetration of the impurity atoms into the Ni crystal

lattice.

It was also found that after the thermal treatment of a film-based alloy based on Fe and Mo ($c_{Fe i} \cong 65$ at. %), in the diffraction patterns along with the lines corresponding to the bcc-Fe phase, new lines appear from the crystallographic planes of the metastable phase Fe$_2$Mo, oxides Fe$_3$O$_4$, Fe$_2$O$_3$ and bcc-Mo phase.

The longitudinal strain coefficient is 4 to 6 units, which is two times less compared to double- and three-layer film systems of the same components. This can be explained by the absence in the film alloys of the interface mechanism of scattering conduction electrons between individual layers.

The TCR is not significantly dependent on the components concentration and with a total thickness of the samples from 30 to 60 nm, with an increase in temperature from 300 to 800 K.

AKNOWLEDGEMENTS

СПИСОК ЛІТЕРАТУРИ

1. G.-D. Sim, J.A. Krogstad, K.M. Reddy, K.Y. Xie, G.M. Valentino, T.P. Weihs, K.J. Hemker, *Sci. Adv.* **3**, e1700685 (2017).
2. J. Zhang, J.G. Li, T. Jin, X.F. Sun, Z.Q. Hu, *Mater. Sci. Eng.* A **527**, 3051 (2010).
3. T. Ohgai, Y. Tanaka, R. Washio, *J. Solid State Electrochem.* **17**, 743 (2013).
4. M. Manazoglu, G. Hapci, G. Orhan, *J. Solid State Electrochem.* **20**, 191 (2016).
5. Y. Gu, X. Zhan, Z. Ji, Y. Zhang, *Appl. Surf. Sci.* **252** No 11, 4009 (2006).
6. O.V. Synashenko, O.P. Tkach, I.P. Buryk, L.V. Odnodvorets, S.I. Protsenko, N.I. Shumakova, *Probl. Atomic Sci. Tech.* **6**, 169 (2009).
7. R. Banerjee, C.A. Brice, S. Banerjee, *Mat. Sci. Eng. A* **347**, 1 (2003).
8. S.H. Zhou, Y. Wang, C. Jiang, J.Z. Zhu, L.Q. Chen,

Z.K. Liu, *Mater. Sci. Eng. A* **397**, 288 (2005).
9. L.V. Odnodvorets, N.I. Shumakova, O.P. Tkach, I.Y. Protsenko, *J. Nano- Electron. Phys.* **1,** 1, 29 (2009).
10. P. Kedzierzawski, D. Oleszak, M. Janik-Czachor, *Mater. Sci Eng.* **300**, 105 (2001).
11. V.D. Jović, B.M. Jović, V. Lačnjevac, G. Branković, S. Bernik, A. Rečnik, *Electrochim. Acta* **55**, 4188 (2010).
12. A.G. Bagmut, I.G. Shipkova, V.A. Zhuchkov, *Func. Mater.* **16** No 2, 161 (2009).
13. I.P. Buryk, L.V. Odnodvorets, *J. Nano- Electron. Phys.* **1** No 3, 20 (2009).
14. T.M. Grychanovs'ka, V.V. Bibyk, I.P. Buryk, O.S. Gryschuk, L.A. Sheshenya, *J. Nano- Electron. Phys.* **5** No 1, 01014 (2013).
15. M.J. Benitez, D. Mishra, P. Szary, G.A. Badini Confalonieri, M. Feyen, A.H. Lu, L. Agudo, G. Eggeler, O. Petracic and H. Zabel, *J. Phys. Condens. Matter.* **23**, 126003 (2011)